Am J Clin Exp Urol 2021;9(1):18-31
www.ajceu.us /ISSN:1943-8141/AJCEU0121754

Original Article

Platelet TSP-1 controls prostate cancer-induced osteoclast differentiation and bone marrow-derived cell mobilization through TGFβ-1

Bethany A Kerr[1,2], Koran S Harris[1], Lihong Shi[1], Jeffrey S Willey[3], David R Soto-Pantoja[1,3,4], Tatiana V Byzova[5,6]

[1]Department of Cancer Biology and Comprehensive Cancer Center, Wake Forest School of Medicine, Winston-Salem, NC, USA; [2]Department of Orthopaedic Surgery, Wake Forest School of Medicine, Winston-Salem, NC, USA; [3]Department of Radiation Oncology and Comprehensive Cancer Center, Wake Forest School of Medicine, Winston-Salem, NC, USA; [4]Department of Surgery, Wake Forest School of Medicine, Winston-Salem, NC, USA; [5]Department of Molecular Cardiology, Joseph J. Jacobs Center for Thrombosis and Vascular Biology, Lerner Research Institute, Cleveland Clinic, Cleveland, OH, USA; [6]Taussig Cancer Center, Cleveland Clinic, Cleveland, OH, USA

Received September 4, 2020; Accepted December 24, 2020; Epub February 15, 2021; Published February 28, 2021

Abstract: The development of distant metastasis is the leading cause of prostate cancer (CaP)-related death, with the skeleton being the primary site of metastasis. While the progression of primary tumors and the growth of bone metastatic tumors are well described, the mechanisms controlling pre-metastatic niche formation and homing of CaP to bone remain unclear. Through prior studies, we demonstrated that platelet secretion was required for ongoing tumor growth and pre-metastatic tumor-induced bone formation. Platelets stimulated bone marrow-derived cell (BMDC) mobilization to tumors supporting angiogenesis. We hypothesized that proteins released by the platelet α granules were responsible for inducing changes in the pre-metastatic bone niche. We found that the classically anti-angiogenic protein thrombospondin (TSP)-1 was significantly increased in the platelets of mice with RM1 murine CaP tumors. To determine the role of increased TSP-1, we implanted tumors in TSP-1 null animals and assessed changes in tumor growth and pre-metastatic niche. TSP-1 loss resulted in increased tumor size and enhanced angiogenesis by immunohistochemistry. Conversely, TSP-1 deletion reduced BMDC mobilization and enhanced osteoclast formation resulting in decreased tumor-induced bone formation as measured by microcomputed tomography. We hypothesized that changes in the pre-metastatic niche were due to the retention of TGF-β1 in the platelets of mice after TSP-1 deletion. To assess the importance of platelet-derived TGF-β1, we implanted RM1 CaP tumors in mice with platelet factor 4-driven deletion of TGF-β1 in platelets and megakaryocytes. Like TSP-1 deletion, loss of platelet TGF-β1 resulted in increased angiogenesis with a milder effect on tumor size and BMDC release. Within the bone microenvironment, platelet TGF-β1 deletion prevented tumor-induced bone formation due to increased osteoclastogenesis. Thus, we demonstrate that the TSP-1/TGF-β1 axis regulates pre-metastatic niche formation and tumor-induced bone turnover. Targeting the platelet release of TSP-1 or TGF-β1 represents a potential method to interfere with the process of CaP metastasis to bone.

Keywords: Prostate cancer, bone metastasis, platelets, thrombospondin, transforming growth factor-beta, angiogenesis

Introduction

An estimated 191,930 men will be diagnosed with prostate cancer (CaP) in 2020, surpassing lung cancer incidence [1]. Early detection has improved 5-year survival rates to 100 percent with a local diagnosis. However, men diagnosed with distant CaP metastases face a 30 percent chance of survival at five years, with bone being the most common site of CaP metastasis [1]. 90% of CaP patients display skeletal metastases at autopsy regardless of prior bone symptom reporting. While the effects of CaP tumor growth in bone have been studied, CaP metastasis mechanisms to skeletal tissues remain unclear. Our previous findings demonstrated

cross-talk between the tumor and bone before metastasis, which may account for the propensity of CaP to metastasize to the skeleton [2-4]. Also, this communication indicated the preparation of a pre-metastatic niche for circulating tumor cells.

Possible communication mechanisms between the primary tumor and bone include proteins, RNAs, and mRNAs circulating in plasma, within platelets, or attached to sentinel tumor cells. Platelets function in metastasis by aggregating with tumor cells, coating circulating tumor cells as protection from immune recognition, promoting tumor cell adhesion and growth, enhancing angiogenesis, and stabilizing tumor vasculature [5-9]. In the primary tumor, platelets promote tumor stability and metastasis by direct interaction with tumor cells, with the tumor vasculature, and through secreted cytokines [10]. During tumor progression to metastasis, our studies have shown that platelets are required for increased bone formation stimulated by primary tumor growth [3] and also for mobilization of bone marrow-derived cells (BMDCs) from the bone marrow [4]. Platelets contain many pro-angiogenic and anti-angiogenic factors: thrombospondin (TSP)-1, vascular endothelial growth factor (VEGF), transforming growth factor (TGF)-β1. Importantly, platelets have selective separation, uptake, and release of pro- and anti-angiogenic proteins [11-13]. Platelets also secrete proteins capable of altering bone turnover, such as matrix metalloproteinase (MMP)-9, cathepsin K, tartrate-resistant acid phosphatase (TRAP), receptor activator of NF-κB ligand (RANKL), and osteoprotegerin. Thus, platelet-derived proteins may play an active role in tumor progression and the development of distant metastases.

Platelet-sequestered TSP-1 controls both bone turnover and CaP progression. In lung and breast cancers, TSP-1 promotes tumor cell metastasis and adhesion [14, 15], with one of the studies demonstrating that cell metastasis due to TSP-1 is dependent upon platelets [14]. In breast cancer patients, TSP-1 levels in the plasma correlate directly with cancer progression and severity [16]. Functionally, TSP-1 binds latent TGF-β1 and induces its activation [17, 18], which may account for many of TSP-1's effects on cancer growth and bone turnover. In CaP, androgen withdrawal causes TSP-1 production in the prostate. While TSP-1 initially reduces tumor progression and vascularization, prolonged TSP-1 exposure results in high VEGF production by CaP cells, and a dependency of the cancer cells on TSP-1 activated TGF-β1 [19, 20]. Thus, castration may stimulate TSP-1-dependent activation of TGF-β1 in prostates promoting the later stages of tumor growth, angiogenesis, and metastasis. TGF-β1 levels in CaP patients are predictive of future biochemical recurrence [21-23] and are elevated in patients with bone metastases [22, 24]. Plasma TGF-β1 levels are primarily due to the release of platelet TGF-β1 during the collection and preparation of blood samples [25], indicating that the TGF-β1 associated with CaP bone metastasis is likely platelet-derived. The utility of platelet TSP-1 and TGF-β1 as cancer biomarkers presents the possibility that these platelet proteins control pre-metastatic niche formation and tumor-induced bone formation.

While TSP-1 and TGF-β1 play essential roles in the growth of primary tumors and bone metastases, the role of the TSP-1/TGF-β1 axis in pre-metastatic tumor communication remains unstudied. In this study, we investigated whether TSP-1 accumulation in platelets affects primary tumor progression and tumor-induced bone formation. We then examined what role the TSP-1 induced activation of TGF-β1 played in these pre-metastatic processes. We demonstrate that the platelet TSP-1/TGF-β1 axis has little effect on primary tumor growth but controls the bone microenvironment's pre-metastatic changes. Thus, targeting TSP-1 and TGF-β1 will have the most impact on preventing bone metastasis rather than inhibiting primary CaP growth.

Materials and methods

Ethics statements

Animal experiments were performed under Cleveland Clinic IACUC approved protocols (2011-0655; 2015-1369). We obtained approval from the Cleveland Clinic Institutional Review Board before initiating blood sample collection from patients undergoing radical prostatectomy at the Cleveland Clinic Glickman Urological and Kidney Institute. A patient consent form was created for the study with clearly stated goals and describing our research's purpose.

Reagents

All chemicals were obtained from Sigma unless otherwise specified. Media were supplied by the Central Cell Services Core of the Lerner Research Institute.

Cell culture

RM1 murine prostate cancer cells (RRID: CVCL_B459) were provided by Dr. W.D. Heston (Cleveland Clinic). These cells were generated from C57BL/6 mice using the mouse prostate reconstitution model with overexpression of *Myc* and *Ras* [26, 27]. RM1 tumors provide insight into aggressive, androgen-independent, and metastatic CaPs [28]. Cells were cultured in RPMI 1640 supplemented with 10% heat-inactivated FBS, 100 U/mL penicillin, 100 µg/mL streptomycin and were regularly passaged by trypsinization (0.05% trypsin, 0.53 mM EDTA).

Tumor cell injection

Mice were maintained on standard chow in standard housing. Age-matched, male 8-12 week old C57BL/6J (WT; RRID: ISMR_JAX:000664), B6.129S2-*Thbs1*^{tm1Hyn}/J (TSP-1 null; RRID: ISMR_JAX:006141) (Jackson Laboratory), PF4-Cre$^{-/-}$ TGF-β1$^{fl/fl}$ (TGF-β1$^{fl/fl}$), or PF4-Cre$^{+/-}$ TGF-β1$^{fl/fl}$ (PF4-Cre^{+}TGF-β1f$^{l/fl}$, a kind gift from Dr. Barry Coller) mice were anesthetized by 100 mg/kg ketamine and 10 mg/kg xylazine injected i.p.. RM1 cells at a concentration of 4×10^5 cells were injected s.c. into the flank of mice on each side. Control mice of each background were injected s.c. in each flank with PBS. Tumors were allowed to grow 12 days before sacrifice.

Plasma and platelet isolation

While mice were anesthetized, the vena cava was exposed, and blood was collected from the vein into an acid-citrate-dextrose (ACD) buffer containing 1 µg/mL prostaglandin E_1 (PGE_1; Sigma). Platelets and plasma were separated from the platelet-rich plasma of blood by gel filtration, as previously described [4]. The activated supernatant was collected by centrifugation after platelets were treated with 100 nM phorbol 12-myristate 13-acetate (PMA) (Sigma), 1 mM protease inhibitors (Roche complete Mini), and 500 µM mouse PAR-4-amide (Bachem) at 37°C for 45 minutes to stimulate the release of granular contents.

Immunoblotting

Activated platelet releasates and platelet lysates were incubated with 5X Lane Marker Reducing sample buffer (Pierce) and boiled at 95°C for 10 min. Samples underwent electrophoresis on a 7% polyacrylamide gel at 100 V for approximately 2 hours. Proteins were transferred to a nitrocellulose membrane at 100 V for 1 hour at 4°C. Membranes were blocked in 10% milk in TBS containing 0.1% Tween-20. TSP-1 antibody (1:1000; Santa Cruz Biotechnology; RRID: AB_831756) was used to detect platelet-derived proteins, with fibrinogen antibody (1:1000; Abcam; RRID: AB_732366) used as a loading control. Horseradish-peroxidase conjugated secondary antibodies (1:5000; BioRad; RRIDs: AB_11125345 and AB_808614) were used with a luminescent substrate (Pierce SuperSignal West Pico) to visualize proteins. NIH Image J (RRID: SCR_003070) was used to quantify band densitometry.

Whole blood analysis

Mice were anesthetized with 10 mg/kg xylazine and 100 mg/kg ketamine. The vena cava of mice was exposed, and blood was collected from the vein into 0.1 mL ACD buffer containing 1 µg/mL PGE_1. Whole blood was subjected to complete blood count (CBC) analysis with differential to determine blood cell concentrations using an Advia 120 laser hematology system (Siemens Healthcare Diagnostics) in the Center for Cardiovascular Research at the Lerner Research Institute. White blood cell (WBC) counts, lymphocyte counts, platelet counts, and mean platelet volume (MPV) were assessed.

Tumor analysis

Tumors were removed from the mice upon sacrifice. Tumors were weighed, and the dimensions of the tumors were measured by caliper. Tumor volume was calculated as $(d_1 \times d_2)^{(3/2)} \times (\pi/6)$, as described in [28]. Tumors were then placed in 10% formalin or embedded in OCT for sectioning. Tumors embedded in paraffin were sectioned and stained with hematoxylin and eosin. Tumors embedded in OCT freezing medi-

um were sectioned at 7 μm. Sections were then fixed in 4% PFA and incubated with primary antibodies: anti-CD31 (1:50, BD Pharmigen; RRID: AB_393571), anti-CD42b (1:75, Millipore; RRID: AB_10712312) or anti-smooth muscle actin (SMA, 1:100, Abcam; RRID: AB_2223021). Tissues were then exposed to a fluorescently labeled secondary antibody (Invitrogen). Slides were mounted with Vectamount + DAPI (Vector Labs). Slides were scanned with an Olympus VS110 in the Wake Forest School of Medicine Virtual Pathology Core, and whole tumor staining was analyzed using the Halo Software.

Lymphocyte isolation

Lymphocytes were isolated from whole blood using Ficoll-Paque PLUS (GE Healthcare) according to the manufacturer's procedure. Briefly, whole blood was layered on Ficoll-Paque PLUS and centrifuged at 2000 rpm for 10 minutes without brakes. The lymphocyte layer was removed and washed. Pelleted lymphocytes were resuspended in 2 mL DMEM/F12 and stored at 4°C until staining.

Flow cytometry

Isolated lymphocytes were blocked with 2 μL murine FcR blocking reagent (Pierce) for 15 minutes. Lymphocytes were then incubated with 20 μL of fluorescently conjugated antibodies. Either CD184/CXCR4 conjugated with FITC (R&D Systems; RRID: AB_2091799) or CD117/c-kit conjugated with PE (Miltenyi Biotec; RRID: AB_2660118) were used. Lymphocytes were then washed and resuspended in 1% formalin. Stained lymphocytes were then analyzed using a BD FACS Canto II running the FACS Diva software (RRID: SCR_001456). Fluorescence values of stained lymphocytes were normalized to an isotype control sample.

Microcomputed tomography (MicroCT)

The microCT analysis was performed one day before the injection of tumor cells and after 12 days of tumor growth. Pre-injection scans were performed in live animals with *ex vivo* scans performed at experimental termination on isolated legs in PBS after overnight fixation in 10% formalin. Scans were conducted in the Cleveland Clinic Biomedical Imaging and Analysis Core Center on a GE eXplore Locus microCT (GE Healthcare), and 360 X-ray projections were collected in 1° increments (80 kVp; 500 mA; 26 min total scan time). Projection images were preprocessed and reconstructed into 3-dimensional volumes (1024^3 voxels, 20 μm resolution) on a 4PC reconstruction cluster using a modified tent-FDK cone-beam algorithm (GE reconstruction software). Three-dimensional data was processed and rendered (isosurface/maximum intensity projections) using MicroView (Parallax Innovations). For each volume, a plane perpendicular to the z-axis/tibial shaft was generated and placed at the base of the growth plate. A second, parallel plane was defined 1.0 mm below, and the entire volume was cropped to this volume of interest for quantitative analysis [29]. Image stacks from each volume of interest were exported for quantitative analysis. Cancellous bone masks were generated in MicroView, and 3D trabecular structural indices were extracted using custom MatLab (The MathWorks, Inc; RRID: SCR_001622) algorithms. Trabecular thickness (Tb.Th) and trabecular spacing (Tb.Sp) were determined by previously reported methods. The trabecular number (Tb.N) was calculated by taking the inverse of the average distance between the medial axes of trabecular bone segments. Bone volume fraction (BV/TV, total bone voxels divided by total cancellous bone mask voxels) and bone surface area (BSA, the sum of pixels along edges of trabecular bone) were also calculated for each VOI.

ELISAs

Plasma and activated platelet releasates were subjected to Blue Gene Bone Alkaline Phosphatase, R&D Systems TRANCE/RANKL, or R&D Systems MMP-9 ELISA assays to measure the concentration of proteins. A StanBio Total Calcium LiquiColor Procedure No. 0150 Assay was used to measure calcium levels in the plasma samples. Concentrations were calculated based on a standard curve.

Bone histology

To visualize changes in the bone structure, we isolated the tibiae from mice after microCT scanning. Tibiae were isolated from whole legs, fixed in 10% formalin, and decalcified in 14% neutral buffered EDTA for 10 days. Bones were then washed and dehydrated in serially increasing concentrations of ethanol. Dehydrated

bones were cleared in xylene and embedded in paraffin. Paraffin-embedded bones were sectioned at 5 μm and placed on slides. Sections were stained with hematoxylin and eosin or for 1 hour in the TRAP solution described below. Slides were scanned with the Hamamatsu NanoZoomer by the Virtual Microscopy Core in the Wake Forest School of Medicine. Bone histomorphometry, osteoclast numbers, and growth plate organization were analyzed with the BioQuant Osteo software (RRID: SCR_016423).

Bone marrow isolation and osteoclast differentiation

Tibiae were isolated from mice and the bone marrow extruded. Isolated bone marrow cells were plated at a density of 1×10^6 cells per well in 6 well plates in αMEM media containing 10% FBS, penicillin and streptomycin, and 50 ng/mL MCSF. Seven days later, media was replaced with complete αMEM treated with 25 ng/mL murine MCSF and 30 ng/mL RANKL (R&D Systems) to induce osteoclastogenesis. Media with treatments were changed every few days for 2-3 wks.

TRAP staining

Tartrate-resistant acid phosphatase (TRAP) staining was performed to determine the number of multinucleated osteoclasts formed from isolated bone marrow macrophage cells. Cells were washed and fixed in a 10% glutaraldehyde solution for 15 min at 37°C. Cells were then incubated with a TRAP staining solution (0.3 mg/mL Fast Red Violet LB, 0.05 M sodium acetate, 0.03 M sodium tartrate, 0.05 M acetic acid, 0.1 mg/mL naphthol, 0.1% Triton X-100, pH 5.0) for 2 hours at 37°C. Cells were observed using a Leica DMIRB inverted light microscope in the LRI Imaging Core. TRAP-stained cells with at least three nuclei were counted per well and were considered differentiated osteoclasts.

Clinical samples

An approval from the Cleveland Clinic Institutional Review Board was obtained before the initiation of the blood sample and tumor tissue collection from men undergoing radical prostatectomy at the Cleveland Clinic Glickman Urological and Kidney Institute. Tumor sections from each patient were analyzed by a pathologist, and T stages were assigned. Whole blood (3-4 mL) was collected by venipuncture in Na_2EDTA tubes (BD Biosciences) from patients prior to surgery. Plasma and platelets were isolated from whole blood by centrifugation and gel filtration, as previously described [2, 3]. Platelets were activated with 50 μM human TRAP-6-amide (Bachem), 1 mM protease inhibitors, and 100 nM PMA to stimulate granule release. Isolated plasma and platelet releasates from six patients were assayed using the RayBiotech Human TGF-β1 ELISA according to the manufacturer's instructions. Two separate samples from each patient were analyzed and compared to a standard curve to obtain the concentration in pg/mL of each protein in the samples.

Statistical analysis

Student's *t* test analysis or one-way ANOVA analysis with Tukey post-test were used to determine statistical significance using the GraphPad Prism 7.0 software (RRID: SCR_002798). * represents $P<0.05$, ** represents $P<0.01$, *** represents $P<0.005$.

Results

Platelets accumulate TSP-1 during prostate tumor growth

We have previously shown that platelets actively sequester both host- and tumor-derived proteins promoting angiogenesis and bone marrow-derived cell (BMDC) mobilization [2, 4]. Using a syngeneic tumor model, we determined thrombospondin (TSP)-1 levels in platelets of mice bearing RM1 prostate tumors (**Figure 1A**). While TSP-1 levels remained unchanged in plasma, TSP-1 was approximately 6-fold higher in the platelets of mice bearing tumors than controls (**Figure 1B**). A similar upregulation of platelet TSP-1 was found in B16F10 syngeneic melanoma tumor growth [30]. Since TSP-1 is classically anti-angiogenic, we questioned whether this upregulation was solely a host response inhibiting tumor progression or if there was a secondary purpose of this significant upregulation.

TSP-1 inhibits primary tumor growth but stimulates the pre-metastatic bone response

To determine how TSP-1 accumulation affects tumor progression, we implanted murine RM1 prostate tumors in TSP-1 null mice. Even in the

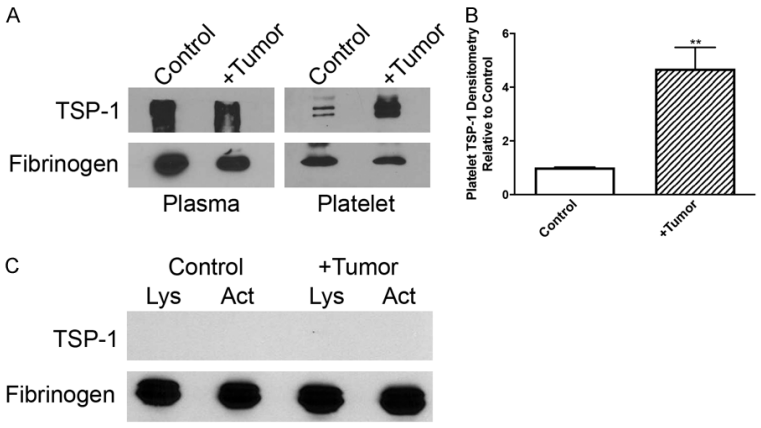

Figure 1. Tumor-bearing mice accumulate platelet TSP-1. (A, B) Activated platelets and plasma from control and RM1 tumor-bearing WT mice were immunoblotted for TSP-1 and fibrinogen (loading control). (B) Densitometry of platelet TSP-1 bands was quantified normalized to loading controls and represented as mean relative to control ± SEM (n=3) ** represents P<0.01 by Student's t test. (C) Activated (Act) or lysed (Lys) platelets from control and RM1 tumor-bearing TSP-1 null mice were immunoblotted for TSP-1 and fibrinogen.

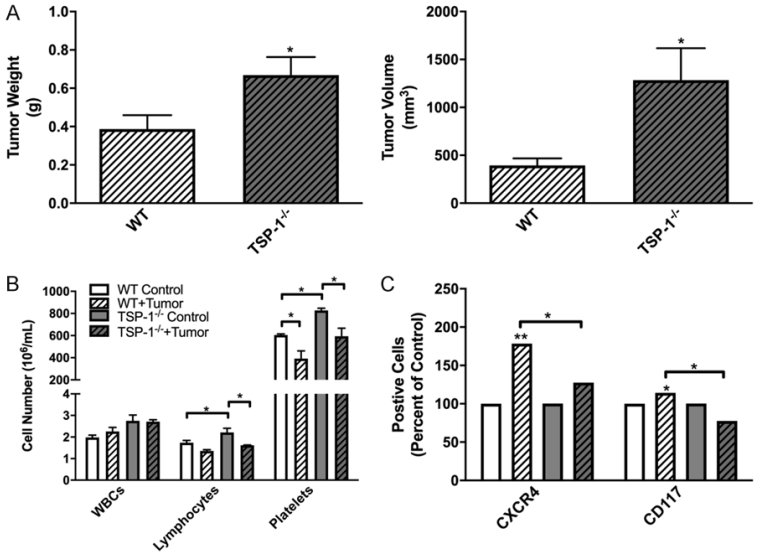

Figure 2. TSP-1 deficiency induces tumor formation but inhibits progenitor cell mobilization. WT and TSP-1 null mice were implanted with RM1 tumors subcutaneously. (A) Tumor weight and volume were measured and represented as mean ± SEM (n=6-8). (B, C) Whole blood was collected and (B) white blood cell (WBC), lymphocytes, and platelet cell numbers were measured and represented as mean cell number ± SEM (n=3). (C) Isolated lymphocytes analyzed by flow cytometry for circulating progenitor cells using the markers CXCR4 and CD117. Quantification of positive cell numbers as mean percent of control ± SEM (n=2-4). * represents P<0.05 and ** represents P<0.01 by Student's t test (A) or one-way ANOVA (B, C).

presence of tumors, no TSP-1 was found in the platelets of TSP-1 null mice (**Figure 1C**). Consistent with previous studies, TSP-1 deletion resulted in significantly larger tumors compared with WT mice (**Figure 2A**). Analysis of cellular blood components demonstrated that TSP-1 deletion results in increased numbers of circulating lymphocytes and platelets (**Figure 2B**) compared with WT mice, consistent with previous studies [31]. Interestingly, the numbers of lymphocytes and platelets were decreased in mice bearing tumors (**Figure 2B**). In previous studies, we have shown that tumor progression is associated with pre-metastatic changes in the bone microenvironment resulting in the release of $CXCR4^+$ BMDCs and bone formation [3, 4]. Also, we previously demonstrated the presence of circulating $CD117^+$ cells in the blood is indicative of cancer progression in CaP patients [32]. Like our previous studies, RM1 tumor implantation in WT mice resulted in increased numbers of circulating $CXCR4^+$ and $CD117^+$ cells (**Figure 2C**). However, although tumors from TSP-1 null mice were significantly larger in this study, we found decreased numbers of $CXCR4^+$ and $CD117^+$ cells in the bloodstream (**Figure 2C**). This paradox indicates that TSP-1 may be anti-tumorigenic locally but promoting pre-metastatic changes in the bone microenvironment.

To further examine the effect of TSP-1 deletion on the primary tumor, we assessed tumor sections for angiogenesis and platelet infiltration. Microvessel area was ~1.3-fold higher in tumors in mice with global TSP-1 deletion (**Figure 3A**) corresponding to the loss of the anti-angiogenic protein. Analysis of mature smooth muscle actin (SMA)-positive blood vessels demonstrated ~2.4-fold increased blood

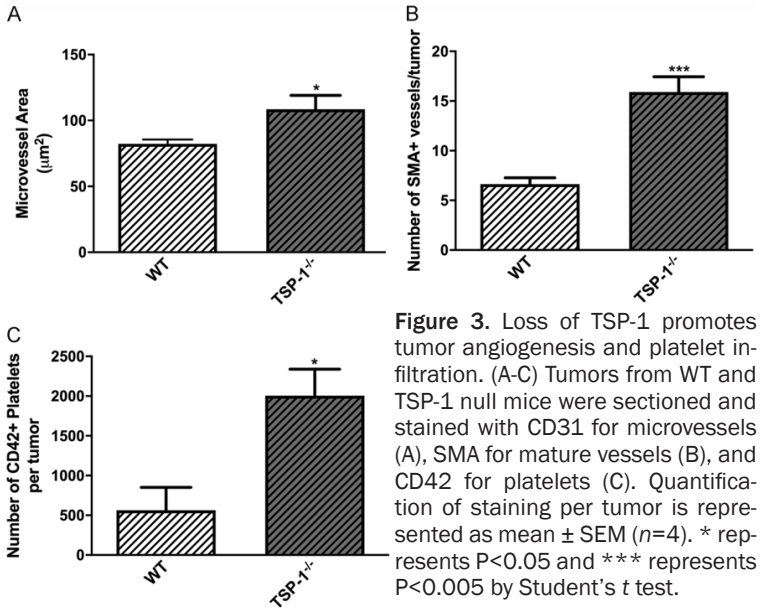

Figure 3. Loss of TSP-1 promotes tumor angiogenesis and platelet infiltration. (A-C) Tumors from WT and TSP-1 null mice were sectioned and stained with CD31 for microvessels (A), SMA for mature vessels (B), and CD42 for platelets (C). Quantification of staining per tumor is represented as mean ± SEM (*n*=4). * represents P<0.05 and *** represents P<0.005 by Student's *t* test.

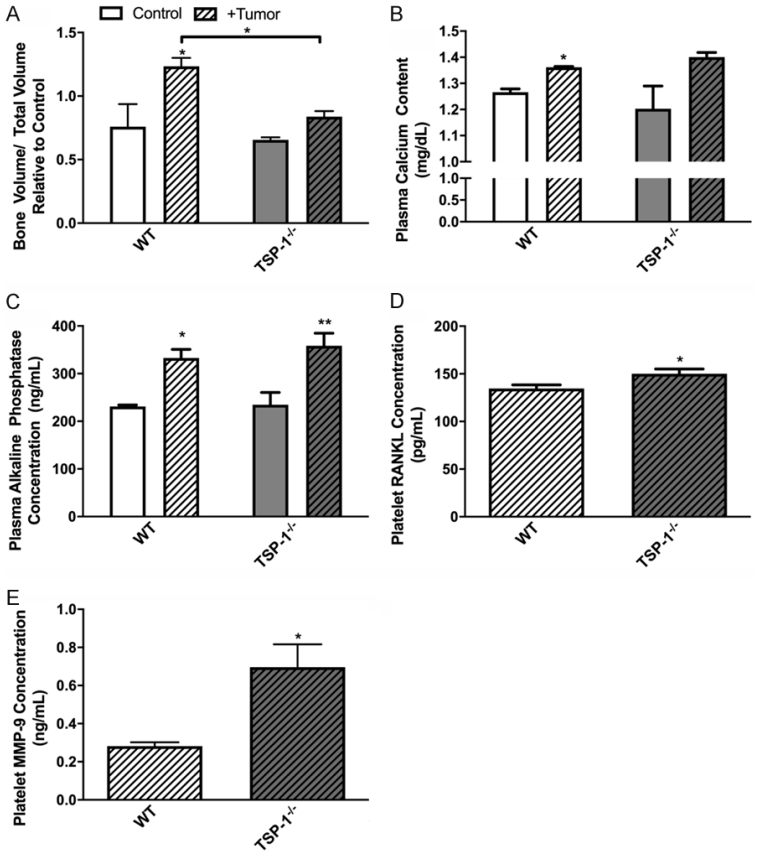

Figure 4. TSP-1 is required for tumor-induced bone formation. (A) Control and RM1 tumor-bearing WT and TSP-1 null mice were analyzed by microCT. The bone volume to total volume ratio was calculated and represented as mean ± SEM (*n*=3-5). (B-E) Plasma and activated platelets were isolated and analyzed by ELISA for protein concentrations of calcium (B), alkaline phosphatase (C), RANKL (D), and MMP-9 (E) represented as mean ± SEM (*n*=3-6). * represents P<0.05 and ** represents P<0.01 by one-way ANOVA (A-C) and Student's *t* test (D, E).

vessel infiltration in tumors from TSP-1 null mice compared with tumors from WT mice (**Figure 3B**). While circulating platelet number was decreased in mice bearing RM1 tumors, the numbers in TSP-1 null mice were not significantly different compared with WT mice (**Figure 2B**). However, within tumors, TSP-1 deletion resulted in ~3.6-fold increased platelet numbers within the tumor (**Figure 3C**). Thus, the increased angiogenesis may permit more platelets to enter tumors, and TSP-1 expression might reduce platelet infiltration.

To evaluate how TSP-1 regulates pre-metastatic niche formation, we analyzed changes in the bone structure by microCT. Pre-metastatic tumor progression stimulates bone formation in WT mice (**Figure 4A**), corresponding to previous studies [3]. However, in TSP-1 null mice, bone formation in response to tumor growth was decreased ~1.5-fold (**Figure 4A**). TSP-1 null mice have mild chondrodysplasia with slightly disorganized columns. However, these changes do not affect the overall bone structure or growth [33]. Interestingly plasma calcium content (**Figure 4B**) and plasma alkaline phosphatase (**Figure 4C**), associated with bone formation, were not significantly different between WT and TSP-1 null mice bearing tumors indicating that osteoblast activity was equal in response to tumor growth. Conversely, platelet RANKL (**Figure 4D**) and MMP-9 (**Figure 4E**) were significantly increased in TSP-1 null mice compared with WT mice bearing tumors, indicating that osteoclast differentiation and function are markedly higher in

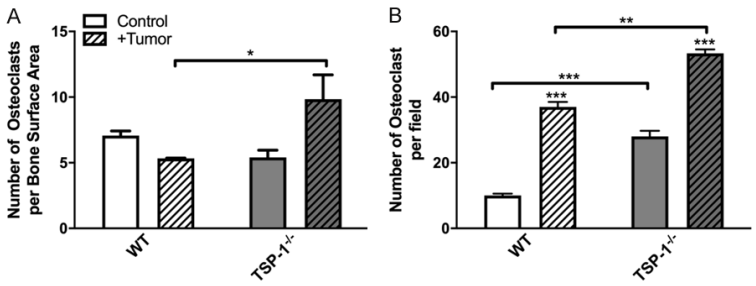

Figure 5. The loss of TSP-1 stimulates osteoclast differentiation. (A) Sections of bones isolated WT and TSP-1 null mice were stained for TRAP expression and the number of osteoclasts per bone surface area calculated and represented as mean ± SEM (*n*=3). (B) Bone marrow macrophages isolated from control and RM1 tumor-bearing WT and TSP-1 null mice were differentiated towards osteoclasts by treatment with MCSF and RANKL. The number of osteoclasts per field was quantified as mean ± SEM (*n*=3). * represents P<0.05, ** represents P<0.01 and *** represents P<0.005 by one-way ANOVA.

TSP-1 null mice. Thus, TSP-1 may be required for the induction of bone formation in response to primary tumor growth.

TSP-1 controls osteoclast differentiation and function in response to tumors

To further examine osteoclast differentiation after TSP-1 deletion, we sectioned bones of WT and TSP-1 null control and tumor-bearing mice and used TRAP staining to enumerate osteoclasts in the bone microenvironment. Quantification of osteoclast numbers demonstrated that TSP-1 null mice bearing tumors had 1.8-fold more osteoclasts on the bone surface compared with WT mice bearing tumors (**Figure 5A**). Also, bone marrow macrophages were isolated from control and tumor-bearing WT and TSP-1 null mice and differentiated *in vitro* into osteoclasts. The TRAP-positive cells with more than three nuclei were considered osteoclasts. Tumor-bearing mice bone marrow macrophages produced 3.7- and 1.9-fold more osteoclasts compared to control WT and TSP-1 null mice, respectively (**Figure 5B**). However, TSP-1 null control mice already contained 2.8-fold more osteoclast progenitors compared with WT (**Figure 5B**). Thus, the deletion of TSP-1 in the bone microenvironment results in increased osteoclast progenitor cells that can then be induced into further differentiation by tumor growth resulting in the prevention of the tumor-induced bone formation seen in WT mice.

Platelet TGF-β1 accumulated with tumor growth and TSP-1 deletion

TSP-1 binds latent TGF-β1 and converts TGF-β1 to its active form [17, 18], particularly during the release of TSP-1 and TGF-β1 by alpha granules during platelet activation [34]. Accordingly, we examined the levels of latent TGF-β1 in platelets isolated from control and tumor-bearing WT and TSP-1 null mice (**Figure 6A**). Platelet TGF-β1 concentration was increased 2.2-fold in WT mice bearing tumors (**Figure 6A**), similar to increases seen in the platelets of advanced CaP patients (**Figure 7**). As expected, TSP-1 deficiency resulted in the accumulation of TGF-β1 in platelets since, without TSP-1, TGF-β1 could not be activated and released [18, 34, 35]. Correspondingly, TSP-1 null mice have reduced active TGF-β1 in their serum and platelets [36]. Platelet TGF-β1 levels were 5.0-fold higher in control TSP-1 null mice compared with WT (**Figure 6A**). Tumor-bearing TSP-1 null mice had 3.0-fold higher platelet TGF-β1 concentrations compared with their WT counterparts (**Figure 6A**).

Platelet TGF-β1 alters angiogenesis and tumor-induced bone formation without affecting primary tumor size

To determine the role of this increased platelet TGF-β1 in tumor progression, we generated megakaryocyte/platelet-specific TGF-β1 knockout mice (PF4-Cre^{+}TGF-β1$^{fl/fl}$) with littermate controls (TGF-β1$^{fl/fl}$). PF4-Cre^{+}TGF-β1$^{fl/fl}$ mice have normal platelet counts and bleeding times [9]. The platelet/megakaryocyte specific deletion results in 93% decreased serum TGF-β1 levels and a 94% decrease in TGF-β1 release from platelets [25]. Tumors implanted in control TGF-β1$^{fl/fl}$ and PF4-Cre^{+}TGF-β1$^{fl/fl}$ grew equally and reached similar volumes (**Figure 6B**). Elevated TGF-β1 levels in the circulation are correlated with increased numbers of circulating tumor cells in the bloodstream [37]. In concert, the deletion of TGF-β1 in platelets resulted in fewer numbers of circulating CXCR4^{+} and CD117^{+} progenitor cells (**Figure 6C**). Angiogenesis, as determined by microvascular

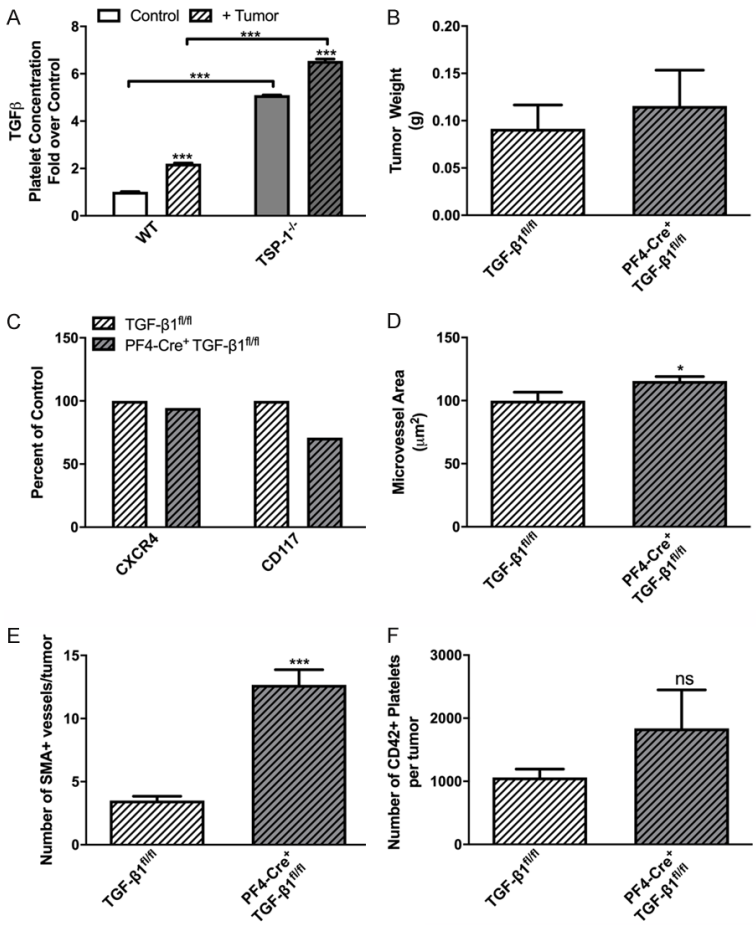

Figure 6. Platelet TGF-β1 is increased in TSP-1 null mice, and its deficiency inhibits progenitor cell mobilization and increases tumor angiogenesis. (A) Platelet TGF-β1 concentration was measured from control and RM1 tumor-bearing WT and TSP-1 null mice and represented as mean ± SEM (*n*=3). (B) RM1 tumors from TGF-β1$^{fl/fl}$ and PF4-Cre^{+}TGF-β1$^{fl/fl}$ mice were weighed and represented as mean ± SEM (*n*=3-11). (C) Whole blood was collected and analyzed by flow cytometry for circulating progenitor cells using the markers CXCR4 and CD117. Representative quantification of positive cell numbers as mean percent of control (*n*=2). (D-F) Tumors were sectioned and stained with CD31 for microvessels (D), SMA for mature vessels (E), and CD42 for platelets (F). Quantification of staining per tumor is represented as mean ± SEM (*n*=4). * represents P<0.05, ** represents P<0.01, and *** represents P<0.005 by one-way ANOVA (A, B) or Student's *t* test (D-F).

area, was slightly increased in tumors from PF4-Cre^{+}TGF-β1$^{fl/fl}$ mice (**Figure 6D**). However, when tumor angiogenesis was examined by counting SMA^{+} mature blood vessels, PF4-Cre^{+}TGF-β1$^{fl/fl}$ tumor displayed 3.6-fold increased vasculature (**Figure 6E**), similar to that seen with TSP-1 deletion (**Figure 3A**). Platelet infiltration was not significantly altered with platelet-specific deletion of TGF-β1 (**Figure 6F**).

Although the deletion of platelet TGF-β1 did not significantly alter primary tumor size, we wanted to assess the effects of platelet-specific TGF-β1 loss on tumor-induced bone formation. As in WT mice, control TGF-β1$^{fl/fl}$ mice displayed increased bone formation in response to tumor growth (**Figure 8A**). The deletion of platelet TGF-β1 prevented tumors of equal size (**Figure 6B**) from stimulating the same increase in bone (**Figure 8A**). This prevention of bone formation was similar to that seen with TSP-1 deletion. Thus, platelet TGF-β1 drives bone formation in response to tumors.

Using the osteoclast differentiation assay on isolated bone marrow macrophages, tumor growth in control TGF-β1$^{fl/fl}$ mice resulted in enhanced numbers of osteoclast precursors (1.3-fold, **Figure 8B**). This effect was magnified another 1.2-fold in platelet TGF-β1 depleted mice (**Figure 8B**), similar to the effect seen with TSP-1 deletion. Correspondingly, the circulating platelet levels of RANKL, which controls osteoclast differentiation, were significantly higher in tumor-bearing mice with platelet TGF-β1 deletion compared with littermate controls (**Figure 8C**). Also, levels of MMP-9, a marker for bone resorption and osteoclast recruitment [38], were increased 1.6-fold in platelet TGF-β1 depleted mice compared with controls (**Figure 8D**). Thus, platelet TGF-β1 is required for tumor-induced bone formation. Since TSP-1 controls TGF-β1 activation and release from platelets, the platelet TSP-1/TGF-β1 axis controls bone turnover and pre-metastatic niche formation in response to primary tumor growth.

Discussion

In this study, we examined the role of platelet TSP-1 in preparing the pre-metastatic niche

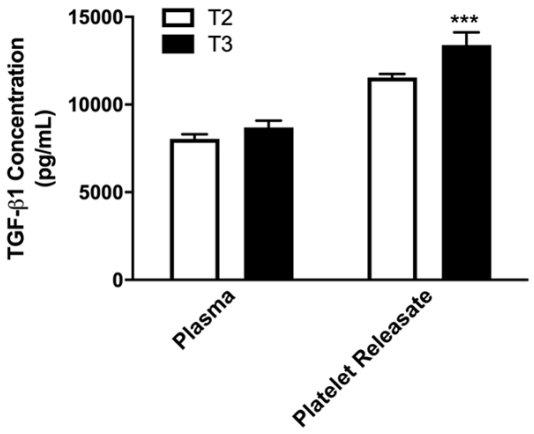

Figure 7. Plasma and platelet TGF-β1 concentration in low and high staged prostate cancer patients. Plasma and activated platelet releasate were isolated from whole blood collected from patients undergoing radical prostatectomy and analyzed by ELISA for mean TGF-β1 concentration ± SEM (*n*=3). T2 represents samples from low stage, less aggressive prostate cancer patients and T3 represents samples from high stage, aggressive prostate cancer patients as determined by a pathologist. *** represents P<0.005 by Student's *t* test.

during CaP progression. Loss of anti-angiogenic TSP-1 resulted in increased primary tumor growth and angiogenesis but prevented tumor communication with the bone microenvironment. Thus, there were decreases in circulating bone marrow-derived progenitor cells and tumor-induced bone formation despite increased primary tumor size. These effects were dependent upon the TSP-1 activation of TGF-β1. Platelet-specific TGF-β1 deletion recapitulated TSP-1 loss, with diminished progenitor cell mobilization and tumor-induced bone formation. With the deletion of total TSP-1 or platelet-specific TGF-β1, osteoclast differentiation was enhanced, tipping the balance away from the tumor-induced bone formation that would otherwise occur. Thus, targeting the TSP-1/TGF-β1 axis may be beneficial in preventing the metastatic progression of CaP.

TSP-1 expression in the primary tumor is associated with diminished tumor growth due to inhibition of angiogenesis. In the early stages of tumor growth, TSP-1 expressed by stromal cells inhibits angiogenesis and tumor growth [39]. Breast cancer-derived tumors in TSP-1 null mice were significantly larger and heavier at 60 and 90 days of growth [40]. Similarly, we demonstrate that CaP tumors are significantly larger in TSP-1 null mice after only 12 days of growth. In the primary tumor, TSP-1 regulates angiogenesis by decreasing neovascularization. Also, TSP-1 is upregulated by the tumor suppressors p53 and PTEN and inhibited by the oncogenes Myc and Ras [41]. The RM1 murine CaP cell line utilized in our studies was generated by Myc and Ras overexpression; however, this does not alter the cell line's ability to express TSP-1 or induce angiogenesis. Our data demonstrate increased angiogenesis and blood vessel maturation in mice with TSP-1 deleted. This enhanced angiogenesis resulted in higher numbers of platelets within tumors. When TGF-β1 was deleted in platelets, angiogenesis increased in tumors. These subcutaneous tumors had significantly higher numbers of mature, SMA covered blood vessels consistent with prior studies showing that platelet-deletion of TGF-β1 results in larger, more mature blood vessels [25]. Changes in tumor angiogenesis and maturation of blood vessels alter the numbers of platelets recruited into tumors.

In the bone microenvironment, the leading metastatic site for CaP, TSP-1 and TGF-β1 are essential signaling proteins controlling bone turnover. TSP-1 deficient mice displayed a higher BV/TV and increased Tb.N than their WT counterparts [42]. While we see a similar increase in the raw data, we normalize our data by comparing mice without and bearing tumors within the same genotype. The change in bone before and after tumor implantation is examined to correct for individual bone structure differences. This manner of presenting the data highlights the effects of tumor implantation on the bone structure. We demonstrate that without tumors, TSP-1 null control mice have a higher number of osteoclasts than WT control mice. These data contrast with a prior study showing equal numbers of osteoclasts in WT and TSP-1 null mice but reduced osteoclast activity demonstrated by serum c-terminal telopeptide crosslinks reduction as a marker of bone resorption [42]. In another study, increased monocyte differentiation occurred in TSP-1 deficient mice [31]. Monocyte differentiation changes likely correlate with changes in cells from the same lineage, namely macrophages and osteoclasts. When tumors were implanted, the numbers of osteoclast progenitors in the bone marrow were enhanced, as demonstrated by increased *ex vivo* differentiation with MCSF

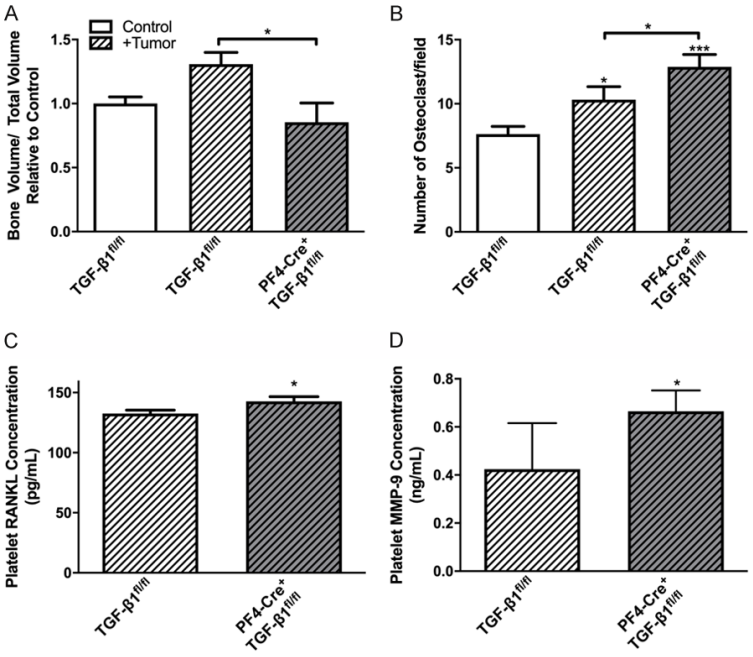

Figure 8. Platelet TGF-β1 is required for tumor-induced bone formation and osteoclast inhibition. (A) Control and RM1 tumor-bearing TGF-β1$^{fl/fl}$ and PF4-Cre^{+}TGF-β1$^{fl/fl}$ mice were analyzed by microCT. The bone volume to total volume ratio was calculated and represented as mean ± SEM (*n*=3). (B) Bone marrow macrophages isolated from control and RM1 tumor-bearing TGF-β1$^{fl/fl}$ and PF4-Cre^{+}TGF-β1$^{fl/fl}$ mice were differentiated towards osteoclasts by treatment with MCSF and RANKL. The number of osteoclasts per field was quantified as mean ± SEM (*n*=16). (C, D) Activated platelets were isolated and analyzed by ELISA for protein concentrations of RANKL (C) and MMP-9 (D) represented as mean ± SEM (*n*=3-6). * represents P<0.05 and *** represents P<0.005 by one-way ANOVA (A, B) and Student's *t* test (C, D).

and RANKL. In the bone marrow, TSP-1 is expressed on the endosteal surface and in megakaryocytes and platelets [43]. On the other side of bone remodeling, TSP-1 induction of activated TGF-β1 induces osteoblast differentiation [44], representing one potential mechanism for the tumor-induced bone formation measured in the control animals. TGF-β1 stimulates early osteoblast proliferation while inhibiting osteoblast activation and bone formation and pushes mesenchymal stem cells towards chondrogenesis or myogenesis over osteogenesis [44]. Thus, alterations of the TSP-1/TGF-β1 signaling axis may regulate bone formation during the development of osteoblastic versus osteoclastic bone lesions in CaP bone metastases.

TSP-1 and TGF-β1 both play integral roles in the interaction between metastatic CaP cells and the bone microenvironment. The co-culture of CaP cells with osteoblasts results in a significant increase in TSP-1 expression [45, 46], while co-culture with prostate stromal cells led to the down-regulation of TSP-1 expression [46]. TGF-β1 regulation of bone cell differentiation and interaction with metastatic cancer cells is well documented. However, the role of TGF-β1 in the initial steps leading to metastasis is controversial and may be dependent on the TGF-β1 concentration and whether bone metastatic lesions are osteoblastic or osteoclastic. In breast cancer, neutralizing TGF-β1 before tumor implantation reduced the number and size of bone lesions and the associated osteolysis due to alterations in myeloid progenitor differentiation into osteoclasts [47, 48]. Neutralization of TGF-β1 resulted in decreased osteoclast number and function in both control and tumor-bearing animals, which is the opposite of our study's findings. However, this neutralization would be more similar to a total knockout of TGF-β1. At the same time, our data results from TGF-β1 deletion in megakaryocytes and platelets alone, leaving the expression of TGF-β1 by other bone microenvironmental cells. Conversely, silencing TGF-β1 in CaP cells reduced the incidence of osteoblastic lesions [49]. Our data demonstrate that TGF-β1 loss in myeloid-derived megakaryocytes and platelets increases osteoclastogenesis and tipping the balance away from bone formation, which may decrease the number of osteoblastic lesions. Supporting the role of the TSP-1/TGF-β1 axis in CaP-induced osteoclastogenesis, TGF-β1 treatment of C4-2B human CaP cells induced RANKL production likely stimulating osteoclast differentiation and function [50]. Further, MMP-9 expression by PC3 human CaP cells induces osteoclast recruitment and activation in the bone microenvironment [38]. Our data demonstrate increased platelet concentrations of MMP-9 and RANKL in mice bearing CaP tumors after

either total TSP-1 deletion or platelet-specific deletion of TGF-β1. Increases in either of these two proteins may cause the enhanced osteoclastogenesis in mice bearing CaP tumors. Thus, the effect of TSP-1 induction on TGF-β1 activation and bone metastasis is likely dependent on whether cancer induces osteoclastic or osteoblastic lesions.

In summary, we demonstrate that targeting the TSP-1/TGF-β1 axis may not alter primary tumor growth but could be used to block pre-metastatic communication between the primary tumor and bone microenvironment, possibly preventing metastasis. Reduction of TSP-1 or platelet-derived TGF-β1 stimulated osteoclastogenesis and reduced tumor-induced bone formation, indicating a potential role for the TSP-1/TGF-β1 axis in the development of osteoblastic or mixed CaP lesions. However, examination of bone metastatic CaP would be required to validate this potential role in bone lesion development. Also, targeting platelet-sequestered proteins could decrease the toxicities seen with systemic perturbation of either TSP-1 or TGF-β1. Finally, the presence and concentration of TSP-1 and TGF-β1 in platelets represent a potential biomarker for aggressive cancers, although further studies examining a broader patient population would be required.

Acknowledgements

We thank Miroslava Tischenko, Richard Rozic, and Steven Maximuk for technical assistance. Dr. Barry Coller of Rockefeller University provided the PF4-Cre/TGFβ1 floxed mice. Dr. Amit Vasanji developed the software and techniques for microCT analysis. This work was supported by research funding from the National Cancer Institute at the National Institutes of Health (grant number CA126847 to TVB). BAK was supported by a Ruth L. Kirschstein NRSA award (grant number CA142133) from the National Cancer Institute at the National Institutes of Health. KSH was supported by an NC A&T NIH/NIGMS MARC U*STAR Grant (T34 GM083980-08) and the DOD PCRP NC Summer Research Program (W81XWH-16-1-0351). The Cleveland Clinic Biomedical Imaging and Analysis Core is funded in part by a NIAMS Core Center Grant P30 AR-050953. The Wake Forest School of Medicine Virtual Pathology Core is funded in part by an NIH/NCATS Grant UL1 TR001420. The funders had no role in the research conducted.

Disclosure of conflict of interest

None.

Address correspondence to: Dr. Bethany A Kerr, Department of Cancer Biology and Comprehensive Cancer Center, Wake Forest School of Medicine, Medical Center Blvd, Winston-Salem 27157, NC, USA. Tel: 336-716-0320; Twitter: @BethanyKerrLab; E-mail: bkerr@wakehealth.edu

References

[1] Siegel RL, Miller KD and Jemal A. Cancer statistics, 2020. CA Cancer J Clin 2020; 70: 7-30.
[2] Kerr BA, Miocinovic R, Smith AK, Klein EA and Byzova TV. Comparison of tumor and microenvironment secretomes in plasma and in platelets during prostate cancer growth in a xenograft model. Neoplasia 2010; 12: 388-96.
[3] Kerr BA, McCabe NP, Feng W and Byzova TV. Platelets govern pre-metastatic tumor communication to bone. Oncogene 2013; 32: 4319-24.
[4] Feng W, Madajka M, Kerr BA, Mahabeleshwar GH, Whiteheart SW and Byzova TV. A novel role for platelet secretion in angiogenesis: mediating bone marrow-derived cell mobilization and homing. Blood 2011; 117: 3893-902.
[5] Borsig L. The role of platelet activation in tumor metastasis. Expert Rev Anticancer Ther 2008; 8: 1247-55.
[6] Gasic GJ, Gasic TB and Stewart CC. Antimetastatic effects associated with platelet reduction. Proc Natl Acad Sci U S A 1968; 61: 46-52.
[7] Jain S, Harris J and Ware J. Platelets: linking hemostasis and cancer. Arter Thromb Vasc Biol 2010; 30: 2362-7.
[8] Kisucka J, Butterfield CE, Duda DG, Eichenberger SC, Saffaripour S, Ware J, Ruggeri ZM, Jain RK, Folkman J and Wagner DD. Platelets and platelet adhesion support angiogenesis while preventing excessive hemorrhage. Proc Natl Acad Sci U S A 2006; 103: 855-60.
[9] Labelle M, Begum S and Hynes RO. Direct signaling between platelets and cancer cells induces an epithelial-mesenchymal-like transition and promotes metastasis. Cancer Cell 2011; 20: 576-90.
[10] Sharma D, Brummel-Ziedins KE, Bouchard BA and Holmes CE. Platelets in tumor progression: a host factor that offers multiple potential targets in the treatment of cancer. J Cell Physiol 2014; 229: 1005-15.
[11] Battinelli EM, Markens BA and Italiano JE. Release of angiogenesis regulatory proteins from platelet alpha granules: modulation of physiologic and pathologic angiogenesis. Blood 2011; 118: 1359-69.

[12] Jonnalagadda D, Izu LT and Whiteheart SW. Platelet secretion is kinetically heterogeneous in an agonist-responsive manner. Blood 2012; 120: 5209-16.
[13] Kamykowski J, Carlton P, Sehgal S and Storrie B. Quantitative immunofluorescence mapping reveals little functional coclustering of proteins within platelet alpha-granules. Blood 2011; 118: 1370-3.
[14] Tuszynski GP, Gasic TB, Rothman VL, Knudsen KA and Gasic GJ. Thrombospondin, a potentiator of tumor cell metastasis. Cancer Res 1987; 47: 4130-3.
[15] Wang TN, Qian X, Granick MS, Solomon MP, Rothman VL, Berger DH and Tuszynski GP. Thrombospondin-1 (TSP-1) promotes the invasive properties of human breast cancer. J Surg Res 1996; 63: 39-43.
[16] Byrne GJ, Hayden KE, McDowell G, Lang H, Kirwan CC, Tetlow L, Kumar S and Bundred NJ. Angiogenic characteristics of circulating and tumoural thrombospondin-1 in breast cancer. Int J Oncol 2007; 31: 1127-32.
[17] Murphy-Ullrich JE and Poczatek M. Activation of latent TGF-beta by thrombospondin-1: mechanisms and physiology. Cytokine Growth Factor Rev 2000; 11: 59-69.
[18] Murphy-Ullrich JE, Schultz-Cherry S and Höök M. Transforming growth factor-beta complexes with thrombospondin. Mol Biol Cell 1992; 3: 181-8.
[19] Colombel M, Filleur S, Fournier P, Merle C, Guglielmi J, Courtin A, Degeorges A, Serre CM, Bouvier R, Clézardin P and Cabon F. Androgens repress the expression of the angiogenesis inhibitor thrombospondin-1 in normal and neoplastic prostate. Cancer Res 2005; 65: 300-8.
[20] Filleur S, Volpert OV, Degeorges A, Voland C, Reiher F, Clézardin P, Bouck N and Cabon F. In vivo mechanisms by which tumors producing thrombospondin 1 bypass its inhibitory effects. Genes Dev 2001; 15: 1373-82.
[21] Baselga J, Rothenberg ML, Tabernero J, Seoane J, Daly T, Cleverly A, Berry B, Rhoades SK, Ray CA, Fill J, Farrington DL, Wallace LA, Yingling JM, Lahn M, Arteaga C and Carducci M. TGF-beta signalling-related markers in cancer patients with bone metastasis. Biomarkers 2008; 13: 217-36.
[22] Shariat SF, Kim JH, Andrews B, Kattan MW, Wheeler TM, Kim IY, Lerner SP and Slawin KM. Preoperative plasma levels of transforming growth factor beta(1) strongly predict clinical outcome in patients with bladder carcinoma. Cancer 2001; 92: 2985-92.
[23] Shariat SF, Walz J, Roehrborn CG, Zlotta AR, Perrotte P, Suardi N, Saad F and Karakiewicz PI. External validation of a biomarker-based preoperative nomogram predicts biochemical recurrence after radical prostatectomy. J Clin Oncol 2008; 26: 1526-31.
[24] Adler HL, McCurdy MA, Kattan MW, Timme TL, Scardino PT and Thompson TC. Elevated levels of circulating interleukin-6 and transforming growth factor-beta1 in patients with metastatic prostatic carcinoma. J Urol 1999; 161: 182-7.
[25] Meyer A, Wang W, Qu J, Croft L, Degen JL, Coller BS and Ahamed J. Platelet TGF-β1 contributions to plasma TGF-β1, cardiac fibrosis, and systolic dysfunction in a mouse model of pressure overload. Blood 2012; 119: 1064-74.
[26] Baley PA, Yoshida K, Qian W, Sehgal I and Thompson TC. Progression to androgen insensitivity in a novel in vitro mouse model for prostate cancer. J Steroid Biochem Mol Biol 1995; 52: 403-13.
[27] Thompson TC, Southgate J, Kitchener G and Land H. Multistage carcinogenesis induced by ras and myc oncogenes in a reconstituted organ. Cell 1989; 56: 917-30.
[28] Voeks DJ, Martiniello-Wilks R and Russell PJ. Derivation of MPR and TRAMP models of prostate cancer and prostate cancer metastasis for evaluation of therapeutic strategies. Urol Oncol 2002; 7: 111-8.
[29] Hildebrand T, Laib A, Muller R, Dequeker J and Ruegsegger P. Direct three-dimensional morphometric analysis of human cancellous bone: microstructural data from spine, femur, iliac crest, and calcaneus. J Bone Min Res 1999; 14: 1167-74.
[30] Zaslavsky A, Baek KH, Lynch RC, Short S, Grillo J, Folkman J, Italiano JE Jr and Ryeom S. Platelet-derived thrombospondin-1 is a critical negative regulator and potential biomarker of angiogenesis. Blood 2010; 115: 4605-13.
[31] Lawler J, Sunday M, Thibert V, Duquette M, George EL, Rayburn H and Hynes RO. Thrombospondin-1 is required for normal murine pulmonary homeostasis and its absence causes pneumonia. J Clin Invest 1998; 101: 982-92.
[32] Kerr BA, Miocinovic R, Smith AK, West XZ, Watts KE, Alzayed AW, Klink JC, Mir MC, Sturey T, Hansel DE, Heston WD, Stephenson AJ, Klein EA and Byzova TV. $CD117^+$ cells in the circulation are predictive of advanced prostate cancer. Oncotarget 2015; 6: 1889-97.
[33] Posey KL, Hankenson K, Veerisetty AC, Bornstein P, Lawler J and Hecht JT. Skeletal abnormalities in mice lacking extracellular matrix proteins, thrombospondin-1, thrombospondin-3, thrombospondin-5, and type IX collagen. Am J Pathol 2008; 172: 1664-74.
[34] Blakytny R, Ludlow A, Martin GE, Ireland G, Lund LR, Ferguson MW and Brunner G. Latent TGF-beta1 activation by platelets. J Cell Physiol 2004; 199: 67-76.

[35] Schultz-Cherry S and Murphy-Ullrich JE. Thrombospondin causes activation of latent transforming growth factor-beta secreted by endothelial cells by a novel mechanism. J Cell Biol 1993; 122: 923-32.
[36] Ahamed J, Janczak CA, Wittkowski KM and Coller BS. In vitro and in vivo evidence that thrombospondin-1 (TSP-1) contributes to stirring- and shear-dependent activation of platelet-derived TGF-beta1. PLoS One 2009; 4: e6608.
[37] Divella R, Daniele A, Savino E, Palma F, Bellizzi A, Giotta F, Simone G, Lioce M, Quaranta M, Paradiso A and Mazzocca A. Circulating levels of transforming growth factor-betaeta (TGF-beta) and chemokine (C-X-C motif) ligand-1 (CXCL1) as predictors of distant seeding of circulating tumor cells in patients with metastatic breast cancer. Anticancer Res 2013; 33: 1491-7.
[38] Dong Z, Bonfil RD, Chinni S, Deng X, Trindade Filho JC, Bernardo M, Vaishampayan U, Che M, Sloane BF, Sheng S, Fridman R and Cher ML. Matrix metalloproteinase activity and osteoclasts in experimental prostate cancer bone metastasis tissue. Am J Pathol 2005; 166: 1173-86.
[39] Kazerounian S, Yee KO and Lawler J. Thrombospondins in cancer. Cell Mol Life Sci 2008; 65: 700-12.
[40] Yee KO, Connolly CM, Duquette M, Kazerounian S, Washington R and Lawler J. The effect of thrombospondin-1 on breast cancer metastasis. Breast Cancer Res Treat 2009; 114: 85-96.
[41] Ren B, Yee KO, Lawler J and Khosravi-Far R. Regulation of tumor angiogenesis by thrombospondin-1. Biochim Biophys Acta 2006; 1765: 178-88.
[42] Amend SR, Uluckan O, Hurchla M, Leib D, Veis Novack D, Silva M, Frazier W and Weilbaecher KN. Thrombospondin-1 regulates bone homeostasis through effects on bone matrix integrity and nitric oxide signaling in osteoclasts. J Bone Miner Res 2015; 30: 106-15.
[43] Kopp HG, Hooper AT, Broekman MJ, Avecilla ST, Petit I, Luo M, Milde T, Ramos CA, Zhang F, Kopp T, Bornstein P, Jin DK, Marcus AJ and Rafii S. Thrombospondins deployed by thrombopoietic cells determine angiogenic switch and extent of revascularization. J Clin Invest 2006; 116: 3277-91.
[44] Bailey Dubose K, Zayzafoon M and Murphy-Ullrich JE. Thrombospondin-1 inhibits osteogenic differentiation of human mesenchymal stem cells through latent TGF-beta activation. Biochem Biophys Res Commun 2012; 422: 488-93.
[45] Zhang X, Kazerounian S, Duquette M, Perruzzi C, Nagy JA, Dvorak HF, Parangi S and Lawler J. Thrombospondin-1 modulates vascular endothelial growth factor activity at the receptor level. FASEB J 2009; 23: 3368-76.
[46] Zhang S, Wang J, Bilen MA, Lin SH, Stupp SI and Satcher RL. Modulation of prostate cancer cell gene expression by cell-to-cell contact with bone marrow stromal cells or osteoblasts. Clin Exp Metastasis 2009; 26: 993-1004.
[47] Buenrostro D, Kwakwa KA, Putnam NE, Merkel AR, Johnson JR, Cassat JE and Sterling JA. Early TGF-β inhibition in mice reduces the incidence of breast cancer induced bone disease in a myeloid dependent manner. Bone 2018; 113: 77-88.
[48] Biswas S, Nyman JS, Alvarez J, Chakrabarti A, Ayres A, Sterling J, Edwards J, Rana T, Johnson R, Perrien DS, Lonning S, Shyr Y, Matrisian LM and Mundy GR. Anti-transforming growth factor ss antibody treatment rescues bone loss and prevents breast cancer metastasis to bone. PLoS One 2011; 6: e27090.
[49] Mishra S, Tang Y, Wang L, DeGraffenried L, Yeh IT, Werner S, Troyer D, Copland JA and Sun LZ. Blockade of transforming growth factor-beta (TGFbeta) signaling inhibits osteoblastic tumorigenesis by a novel human prostate cancer cell line. Prostate 2011; 71: 1441-54.
[50] Zhang J, Lu Y, Dai J, Yao Z, Kitazawa R, Kitazawa S, Zhao X, Hall DE, Pienta KJ and Keller ET. In vivo real-time imaging of TGF-beta-induced transcriptional activation of the RANK ligand gene promoter in intraosseous prostate cancer. Prostate 2004; 59: 360-9.